JOURNAL OF CATALYSIS 98, 32–50 (1986)

$Co/Mo/Al_2O_3$ Catalyst Structure Determination by EXAFS

II. Mo K-Edge of the Sulfided State

N-S. CHIU, S. H. BAUER, AND M. F. L. JOHNSON*,[1]

*Department of Chemistry, Cornell University, Ithaca, New York 14853; and *ARCO Petroleum Products Company, Harvey Technical Center, Harvey, Illinois 60426*

Received April 2, 1985; revised September 17, 1985

A series of preparations of MoO_3/CoO on high-area alumina HDS catalysts, which were previously investigated by EXAFS in their oxide state, were reduced and sulfided following four distinct protocols, and their Mo K-edge absorption spectra recorded. The location of the K-edges for Mo in distorted O_6 octahedra are ≈8 eV above that of the metal, characteristic of Mo^{6+}. Upon initiation of reduction, the edge moves toward lower voltages and after extended treatment reaches about 1 eV above that of the metal, characteristic of Mo^{4+}. The shape of the near-edge absorption spectra also changes. From the areas of resolved Gaussians one can estimate a first-order rate constant for the conversion of the oxide to the sulfide. The activation energy is approximately 4.8 kcal/mole, and the sticking factor is 0.9 for H_2S onto the dispersed material. The effect of Co is clearly discernible in that it reduces the initial conversion rate. The transformation of the oxide to the sulfide is never complete; a residual of up to 30% of the molybdenums remains bonded to oxygens in the virgin preparations, but on extended use in HDS reactors a somewhat lower fraction of the Mo bonding remains attached to oxygen. There is a higher level of microcrystalline order in the sulfided state than in the calcined preparations where the MoO_6 octahedra are highly dispersed. An initial rapid rise in temperature facilitates MoS_2 growth; so does higher Mo loading, but this effect is countered by the presence of Co. In the radial distribution curves, the ratio of peak areas: *A*(Mo–Mo)/*A*(Mo–S) is a measure of MoS_xO_y platelet dimensions. For constant Co it increases with Mo loading; for constant Mo it decreases with Co loading. Structures of freshly sulfided vs HDS-treated catalysts clearly differ in *A*(Mo–Mo)/*A*(Mo–S), and in the effect of Co on that ratio. The EXAFS spectra indicate that details of the treatment as well as the composition determine the *distribution* of platelet sizes in the operating catalysts.

INTRODUCTION

In report I (*1*) we briefly described improved procedures for reducing NEXAFS and EXAFS spectra, and applied these to a series of $Co/Mo/Al_2O_3$ preparations of HDS catalysts in the oxidized state. The radial distribution (RD) curves for highly dispersed molybdenum oxides (on high-area alumina) differ significantly from the RD curves of MoO_3. These data indicate that when the molybdenum loading increased, the *apparent* coordination number of oxygen atoms about Mo decreased, characteristic of major distortions of the MoO_6 octahedra in a manner which differed from that present in MoO_3. The inclusion of cobalt reduced distortions as measured both by the areas of the RD peaks and the resolved shapes of the near-edge absorption functions. For subsequent reference we reproduced in Fig. 1 typical RD curves: *a* (30% MoO_3 + 1.5% CoO) preparation on Catapal, *b* $(NH_4)_6Mo_7O_{24} \cdot 4H_2O$, which most closely, but still only roughly, approximates the precatalyst. In summary:

(i) the distorted MoO_6 octahedra characteristic of a large variety of molybdenum oxides are extensively dispersed on the support;

(ii) the innermost coordination shell consists of some closely bonded oxygen atoms at a mean *R*(Mo–O) ≈ 1.7 Å (peak ψ), with

[1] Present address: 1124 Elder Rd., Homewood, Ill. 60430.

0021-9517/86 $3.00

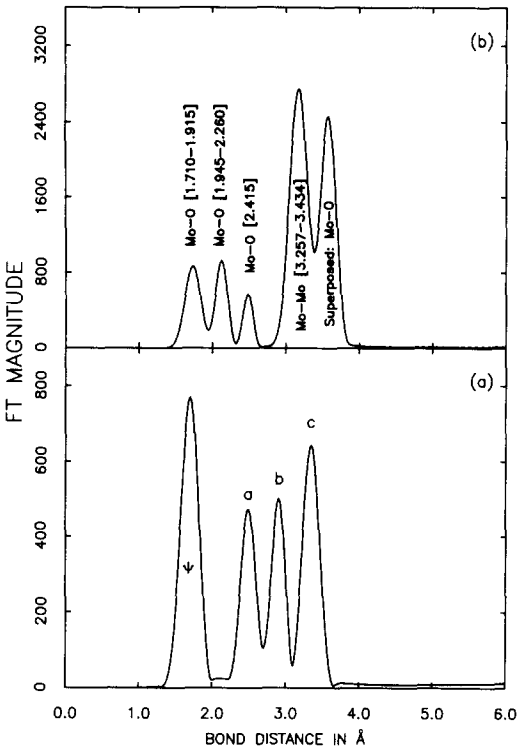

FIG. 1. $D(R)$ curves for: (a) catalyst preparation (30% MoO_3 + 1.5% CoO on high-area alumina); (b) $(NH_4)_6Mo_7O_{24} \cdot 4H_2O$.

the remaining oxygens at a mean R(Mo–O) $\approx$ 2.4 Å. The latter are probably shared with the surface layers of metal atoms of the support (peak *a* in Fig. 1);

(iii) the next coordination shell (peak *b*) may be tentatively assigned to Mo–Al, and peak *c* is due probably to Mo–Mo. The latter indicates that some aggregation of MoO_6 octahedra is present;

(iv) there remains an inherent limitation in the data reduction procedure which prevents assignment of quantitative values to coordination numbers derived from RD peak areas. This appears inescapable as long as no correct atom-form factors for scattering are inserted in the program, because their introduction is inconvenient and their magnitudes are not well established. In particular, when the distances between the central atom and the scatterers in any specified coordination shell covers a range of values (i.e., a highly distorted configuration) the contributed areas of the various atom pairs to the area of the RD peak are significantly less than when the distances are uniform.

A complete listing of the range of compositions used in this study, was presented in our first paper (*1*). The accompanying paper (*2*) consists of a summary of the physical properties of the catalysts and the results of standard activity tests. Here we report structural data derived by applying the improved reduction procedure to NEXAFS and EXAFS spectra of partially and extensively sulfided samples of these preparations, covering a range of H_2S/H_2 time–temperature treatments. The reduced samples may be classified into four categories according to the protocols followed in the conversion of the oxidized to the sulfided states, and their subsequent use in the test reactors. We intended to address the following questions.

(a) Is conversion to MoS_2 complete in the active catalyst?

(b) What are the stages of conversion in the reduction sequence—are there intermediate configurations which are generated and ultimately reduced, or are the Mo–O bonds successively replaced by Mo–S bonds?

(c) How extensive is aggregation of the molybdenum atoms into "rafts" (best described as platelets) of MoS_2?

(d) Do the relative RD peak areas correlate with the various protocols followed in the reduction sequence?

(e) Are there significant structural parameters which correlate with the observed activity tests?

EXPERIMENTS

Three groups of samples (*1*) were reduced by treating the calcined oxides with 10% H_2S/H_2 at atmospheric pressure under a constant flow rate of $\approx$1 liter/h. per gram, following the time sequence programs shown in Fig. 2; test samples were taken at

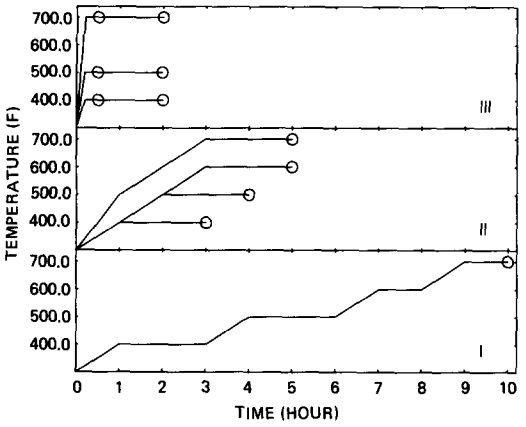

FIG. 2. Temperature–time histograms for sulfiding the various catalyst preparations. All samples were exposed to flowing H_2S (10% in H_2) at 1 atm. Protocol I mimicks the procedure followed in the HDS test reactor. In Protocol III the reactor was preheated to the indicated temperature before the flow of H_2S/H_2 was started.

points designated by ·, and examined at room temperature. Samples subjected to the complete protocol I (at the Harvey Laboratories) were then used for activity tests, and thus exposed to the HDS reaction for extended periods. These catalysts (designated Group IV) were then recovered under an atmosphere of argon and sent to Cornell for examination via EXAFS. They were protected from oxidation not only by the Ar atmosphere but also by the carbon deposit. All other samples were cooled in flowing H_2S/H_2, stored and maintained under argon until their spectra were recorded.

Tests were made to determine how rapidly exposure to the atmosphere leads to significant oxidation, to check on possible failures of the argon cover. A few samples were exposed to air for various times before the scans were taken. No change was observed in their Fourier transforms during the first hour of air exposure at room temperature. Less than 30% of reduction of Mo–S and Mo–Mo peak areas were found after 2 weeks to 3 months of air exposure. Similar effect on Raman spectra were reported by Schrader and Cheng (*3*). Glovebag handling procedures and storage under argon for all the laboratory prepared samples appear to have been adequate.

Groups I and IV include the catalysts with a range of Mo(2–30%) and CoO(0–12%) loading; II and III were limited to 18% MoO_3 with various CoO concentrations. A number of *in situ* scans were made at elevated temperatures with the sample in a heatable mount, under flowing H_2S/H_2; these followed protocols I and III. However, since the time available at the facility was limited, spectra were taken whenever X rays were available, and hence no *in situ* sample could be carried through the entire reduction-time program (I); for III the *in situ* spectra were recorded by taking scans successively from the beginning of heating and H_2S/H_2 gas flow. For comparable treatments we found rather small differences in RD's between *in situ* and laboratory-prepared samples (see below).

Neither free MoO_3 nor bulk crystalline MoS_2 was detected by XRD (estimated <2% crystalline component superposed on amorphous background). Reflectance spectra (prior to sulfiding) showed peaks at 17,200 and 33,300 cm^{-1}; these indicate Co^{2+} and molybdena, respectively. All the EXAFS data were collected at the CHESS Facility, according to the procedure described in report I (*1*), and analyzed as described in detail in Ref. (*4*).

NEAR-EDGE SPECTRA

The Mo absorption edge of precatalysts, in the oxide state is located in the vicinity of 20,010 eV (7.5–9.4 eV above that for Mo metal; the *difference* in edge positions of any specimen and the reference metal is reproducible to 0.5–0.8 eV). This is characteristic of the +VI oxidation state. Upon sulfiding the oxidation states should approach IV in MoS_2; there the K-edge appears at 20,003 eV. We found edge positions for the various samples to range between the lower and upper values. Hence these samples must either incorporate molybdenum in mixed states VI → V → IV, or consist of varying mixtures of VI and IV.

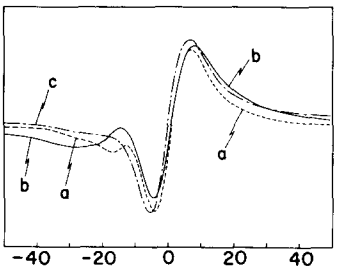

FIG. 3. ESR spectra of three samples. Spectra recorded at room temperature, using a 100-kHz oscillator with midrange field 3606 G; scan range 700 G. (a) 4% MoO_3 on Catapal, sulfided for 10 h (Protocol I); (b) 18% MoO_3 + 6% CoO on Catapal, sulfided for 10 h (Protocol I); (c) 18% MoO_3 + 6% CoO on Catapal, sulfided for ½h (Protocol III).

We observed that the edge position moved relatively rapidly down from 20,010 eV and the shape of the absorption function lost the leading low shoulder (assigned to the $1s$–$4d$ transition) soon after the initiation of sulfiding. Thus, the edge position does not allow us to choose between these two possibilities. It is not unreasonable to assume that in the early stages of reduction molybdenum passes through intermediate oxidation states which have short lifetimes, and only a small fraction become locked in special locations, so that the Mo^V content of the sample as examined is quite low. Support for the presence of Mo^V is provided by ESR signals of moderate intensity, recorded for extensively reduced catalyst preparation (Fig. 3, curves a and b) and one which had been sulfided at about 410°K for only 30 min (curve c). Weaker signals (×0.1) were recorded for the oxide state, and for MoS_2. These tracings are similar to ESR spectra previously reported for sulfided molybdenum catalysts (*5*).

We note that on completion of sulfiding the edge positions of the extensively treated catalysts are 1 eV (sometimes less) above the edge position of MoS_2, but the shape of the absorption functions are similar to that of MoS_2. However, the radial distribution data, summarized below, show that the disappearance of the $1s \rightarrow 4d$ transition shoulder characteristic of the oxide state, does not conclusively prove that all the material was transformed to MoS_2, as had been stated in the literature (*6*). Loss of the shoulder does show that distortions from a trigonal biprism configuration are not large.

Qualitatively, the shapes of the near-edge absorption functions for all the samples can be divided into three types which correlate with the extent of reduction. In the first type (Fig. 4a) the shape is much like that for the oxide catalysts. Only the first few spectra of samples treated *in situ* and sulfided at low temperatures (477°F) for short periods, comprise this group. Their characteristic feature is the prominent shoulder at about 20,002 eV, and flat maximum at about 20,040 eV. As sulfiding progresses, particularly at higher temperatures and longer times, the shoulder fades (Fig. 4b is typical), and the edge moves toward lower energies. Finally, after extensive treatment during HDS processing (Group IV), the near-edge absorption functions (Fig. 4c) attain a shape which is essentially identical with that of MoS_2. These are characterized by a prominent "bump" at ≈20,010 eV and a "droop" at ≈20,040 eV. Preparations with low MoO_3 content (2; 4%) after extended reduction in the laboratory (but no HDS treatment) also have this shape. Masking of the $1s \rightarrow 4d$ shoulder (A_1) in the oxide state by the dominant leading edge of MoS_2 is illustrated in Fig. 4d, which is a record of the absorption function of a mechanical mixture consisting of 6% MoO_3, 12% MoS_2, 82% Al_2O_3.

The near-edge spectra (spanning the energy range 19,970 → 20,040 eV) were resolved into three Gaussians. To achieve the most reliable measures of A_1, A_2, and A_3 (areas of the resolved Gaussians) the identical resolution program was followed for the partially and extended sulfided samples, as for the oxides (*1*). As noted above, A_1 was obscured during the early stages of sulfiding and hence is not readily quantified. While the $1s \rightarrow 4d$ shoulder was still discernible, the area of A_1 did not decrease consistently

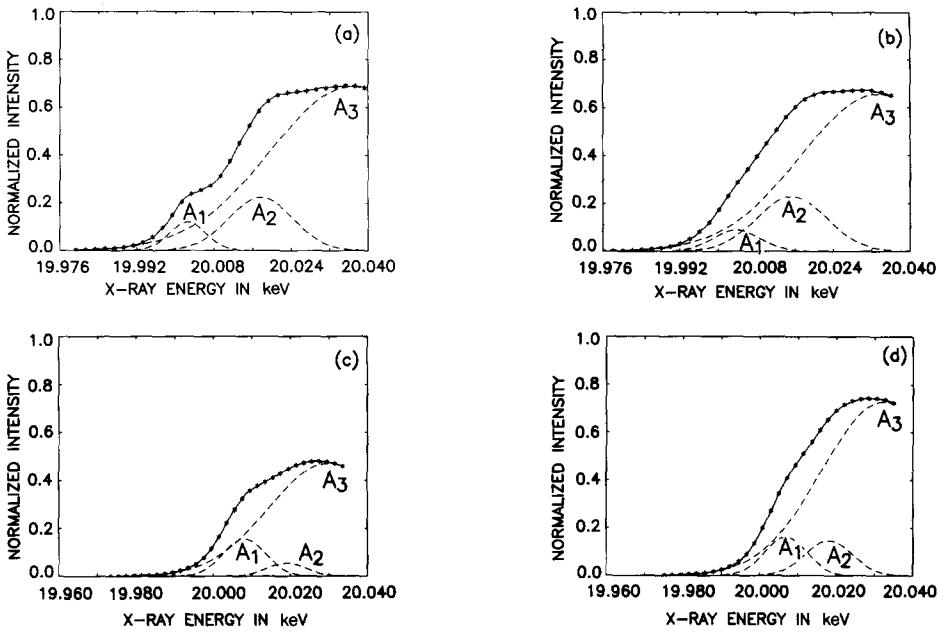

FIG. 4. Near-edge spectra, resolved into three Gaussians. (a) First type (18%/6%). These samples were reduced *in situ* for short periods at 477°K. (b) Similar reductions for longer periods (18%/6%). (c) Is typical of samples of Group IV (catalyst after HDS operation). [Do not be mislead by the lower scales, which are uncalibrated.] (d) Mechanical mixture of MoS_2 and the catalyst preparation (Table 1).

as did A_3. This suggests that the earliest stages of reduction involve oxygens in the first coordination shell which are more distant from Mo, and that the amount of reducible oxygen at any specified temperature is limited. The magnitude of A_2 could not be reliably determined since it is located in a region in which contributions from the tails of adjacent Gaussians overlap. The values of A_3 merit analysis. Protocol III as well as several of the *in situ* runs provided semiquantitative kinetic data.

For every composition, $A_3(t)$ declined from $A_3(0)$ [the oxide], first rapidly and then leveled off, and remained essentially unchanged at $A_3(\infty)$ after 30–120 min at the set temperature; this limiting value depends both on the temperature and composition. As for the oxides, we propose that the magnitude of A_3 is a measure of the distortion of the local field about the Mo atoms; hence it tracks the conversion from the oxide to the sulfide states. At 477°K, after 60 min treatment, $A_3(\infty)$ was attained directly prior to the complete disappearance of the $1s \rightarrow 4d$ shoulder. At higher temperatures, the rate of decline of A_3 was greater and no shoulder could be seen after 20 min. When $A_3(\infty)$ was reached, the leading absorption edges had moved to 20,006 eV (477°K), 20,005 eV (533°K), 20,004 eV (644°K). Further treatment at the indicated temperatures did not significantly change these positions. The change of edge position vs time at different temperatures suggests that the effect of longer treatment may be structural reorganization, rather than reduction. Since the gas-phase composition of 10% H_2S in H_2 was maintained at 1 atm, we assumed that the decline in $A_3(t)$ is a measure of the amount of material reduced, and that it is a first-order process. Hence

$$\ln \frac{A_3(0) - A_3(\infty)}{A_3(t) - A_3(\infty)} = kt, \quad \text{with } k = \Gamma \exp(-\theta/T); \quad (1)$$

with t in seconds. A plot of $\ln k$ vs $1/T$ (Fig. 5)

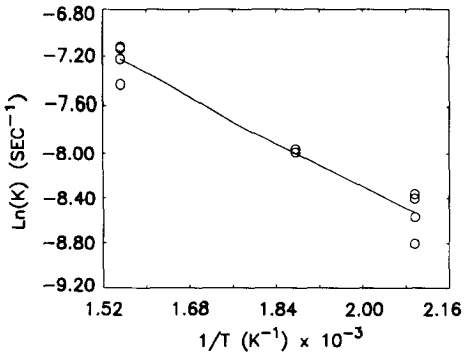

FIG. 5. A plot of ln k vs $1/T$ as defined in Eq. (1).

illustrates the internal consistency of the values deduced for $k(T)$. A least-squares fit [excluding one obviously divergent point] gives $\theta = 2.40 \times 10^3$, equivalent to 4.77 kcal/mole; $\Gamma = 3.05 \times 10^{-2}$. The activation energy is reasonable, as is the preexponential factor. The latter, which is a frequency of conversion per unit of time, corresponds to the number of moles of H_2S which strike unit surface area per second, times the sticking coefficient $\left(\frac{N\bar{c}}{4} \cdot \phi\right)$; $\phi \approx 0.9$.

Values of $A_3(\infty)$ for extensively sulfided samples (Groups I and IV) are plotted in Fig. 6 vs their metal loadings (total moles of metal/100 g of catalysts). These curves show features analogous to the A_3 vs composition curves for the oxide [Ref. (*1*), Fig. 2]. Molybdenum loading increases A_3 in a regular manner, whereas added cobalt reduces its magnitude. Samples which had extended treatment in HDS reactors have somewhat higher A_3 values but the trend with metal loading is unchanged. In the oxide states it was evident that increase in A_3 was associated with increased distortion of the MoO_6 octahedra. We suggest that this interpretation can be carried over to the sulfided states; i.e., increased Mo loading leads to distortion of the field around these atoms but comixed Co lessens this effect.

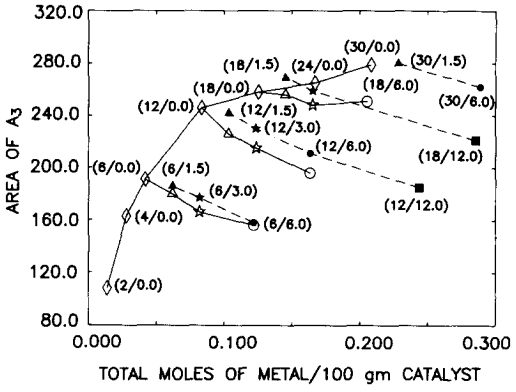

FIG. 6. Dependence of A_3 on total moles of metal/100 g of catalyst. Solid lines connect freshly sulfided samples (Group I); dashed lines connect Group IV samples. ◇, 0% CoO; △, 1.5% CoO; ☆, 3% CoO; ○, 6% CoO; □, 12% CoO.

ABSORPTION DATA (EXTENDED RANGE)

The computed radial distribution functions, $D(R)$ (*1*), for the partially sulfided samples can be more readily interpreted af-

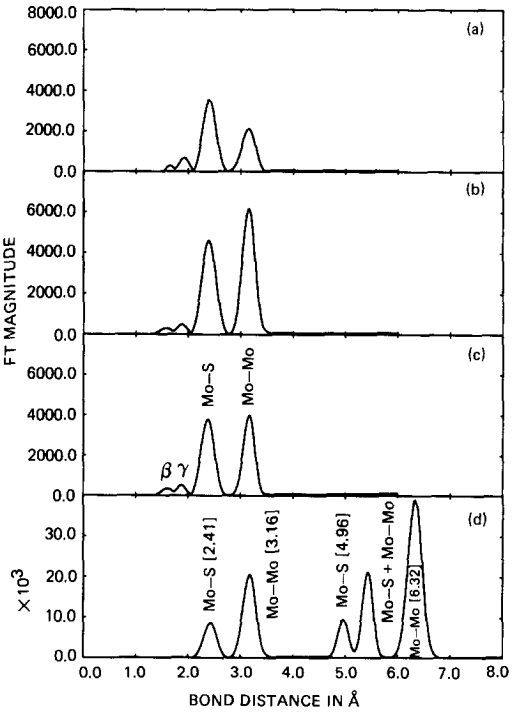

FIG. 7. Typical $D(R)$ curves for extensively reduced preparations (10 h, Protocol I). (a) 2% MoO_3/0% CoO; (b) 18% MoO_3/0% CoO; (c) 18% MoO_3/6% CoO; (d) MoS_2, mechanical mixture with Al_2O_3 (≈50%); note change of vertical scale.

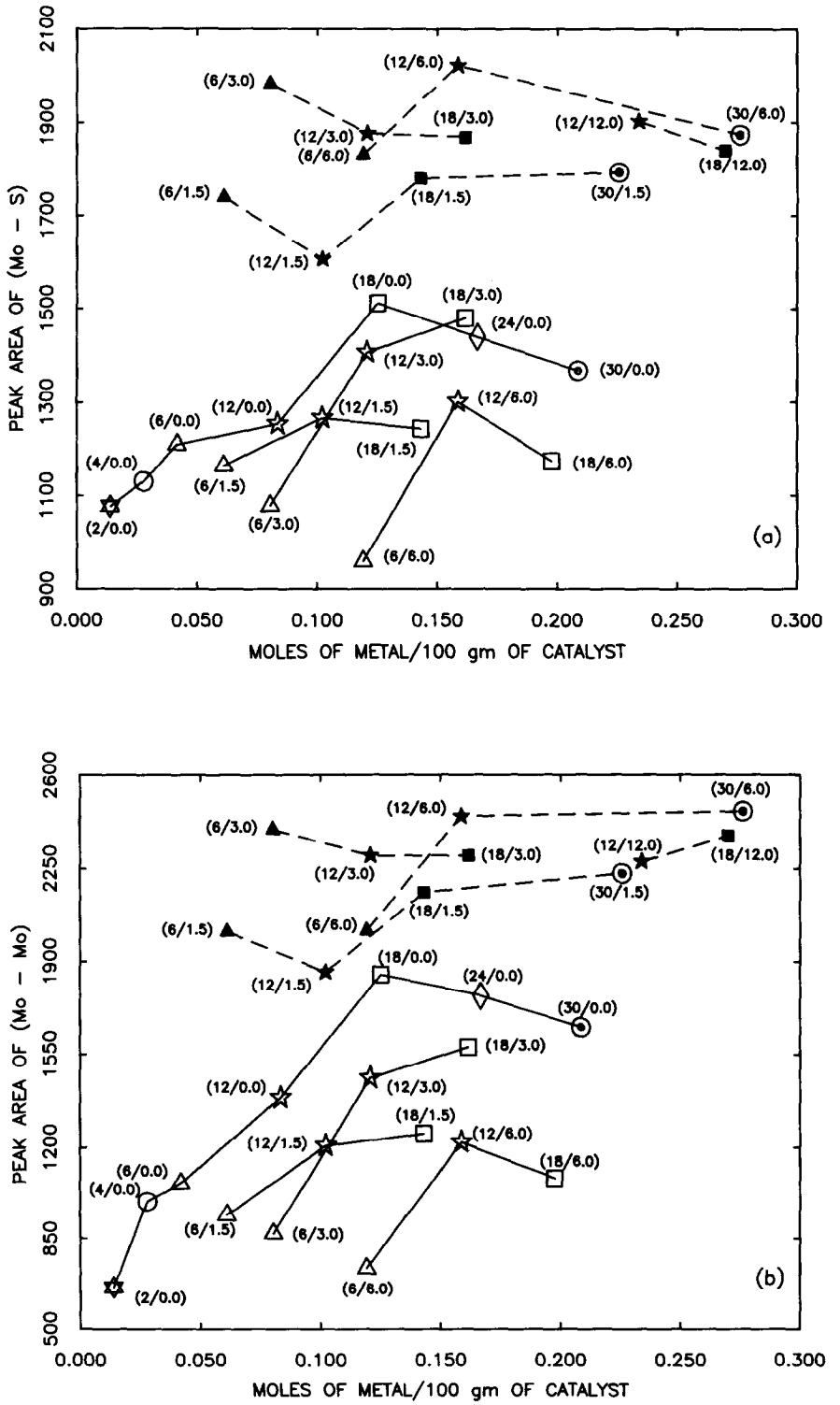

FIG. 8. Areas enclosed by $D(R)$ peaks (Group I). Lower set virgin; upper set after HDS tests. (a) A(Mo–S) vs moles of metal per 100 g of catalyst. (b) A(Mo–Mo) vs moles of metal per 100 g of catalyst. (c) $\Omega \equiv A$(Mo–Mo)/2.393 A(Mo–S) vs moles of metal per 100 g of catalyst.

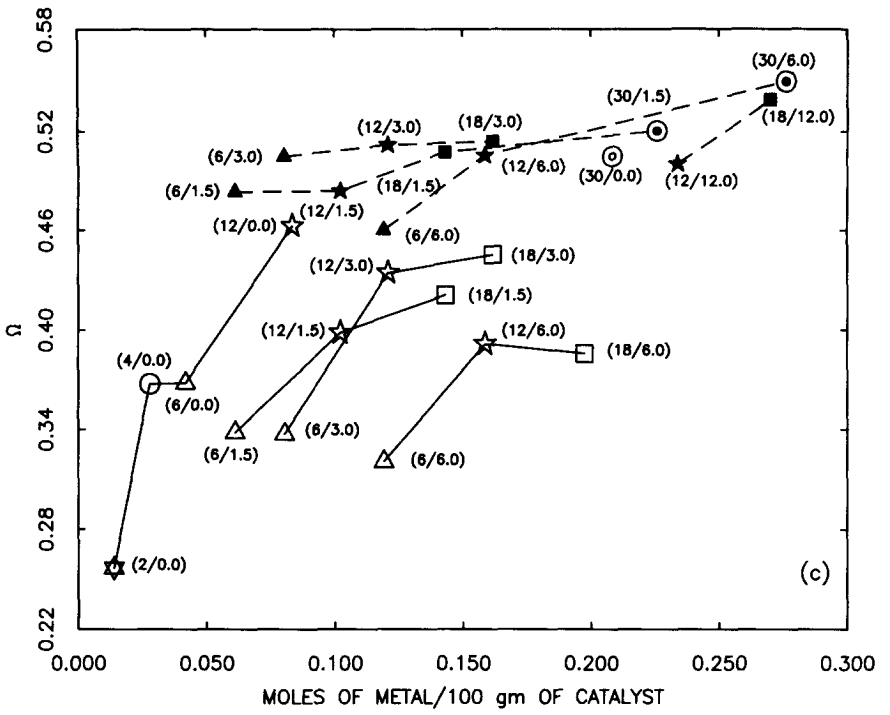

FIG. 8—*Continued.*

ter viewing those for the extensively sulfided preparations. The Group I catalysts, in the oxide form, were treated with H_2S/H_2 for 10 h; the total exposure to H_2S was many times more than is required for stoichiometric conversion to MoS_2. In Fig. 7 typical $D(R)$ curves (2% MoO_3, 0% CoO), (18% MoO_3, 0% CoO), and (18% MoO_3, 6% CoO) are presented. The principal peak appears in the range of 2.34–2.40 Å. It coincides in position with the first peak in the Fourier transform of MoS_2 and arises from backscattering by sulfur atoms in the first coordination shell. However, its area in the catalyst is only about one-half of that in the crystalline sulfide. The second peak, both in MoS_2 and in the extensively sulfided preparation, is attributed to Mo–Mo pairs. For all the fully sulfided samples investigated the areas of the Mo–S, Mo–Mo peaks, and the relative areas, $\Omega = A(\text{Mo–Mo})/[A(\text{Mo–S}) * 2.393]$, are plotted against the number of moles of metal per 100 g of catalyst in Figs. 8a, b, c, respectively. For comparison, in crystalline MoS_2, the defined ratio of areas $\Omega = 1$, since A(Mo–S) = 2648, A(Mo–Mo) = 6337, and their ratio is 2.393.

In Fig. 7 two small peaks appear to the left of the principal Mo–S peak. For reference these are labeled β and γ to distinguish them from peak ψ, which is the main Mo–O peak in the oxide state. Peak β is located at 1.54–1.62 Å and γ at 1.84–1.92 Å; these replace ψ as sulfiding progresses. Peaks β and γ are small and appear in a high-noise region of the radial distribution curve; the background is due to the difficulty in eliminating false peaks ($R < 1.0$ Å) during the data manipulation procedure.

Group IV samples. These radial distributions are similar to Group I except that the areas under the (Mo–S) and (Mo–Mo) peaks are larger, indicating that reorganization into MoS_2-type crystals (and possibly further sulfiding of long Mo–O bonds) continued during extended HDS processing in the test reactors. Note the sequential increase in Ω, as illustrated by Fig. 9a (lab.-sulfided); Fig. 9b, laboratory-sulfided fol-

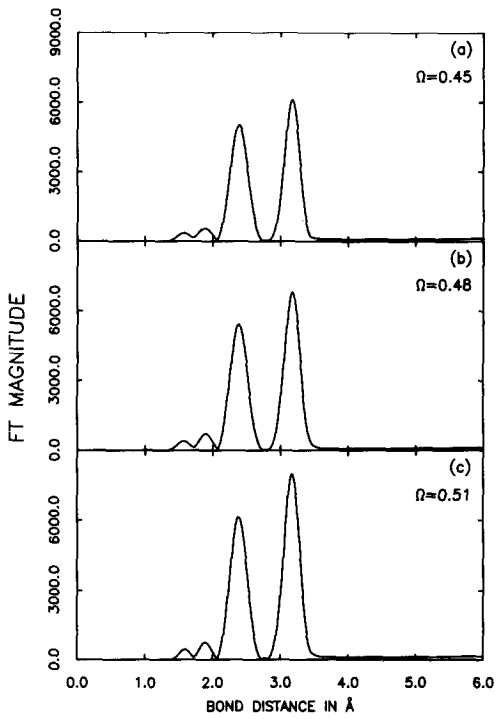

FIG. 9 $D(R)$ curves for Group IV of (18% /3%) which illustrate continued MoS_2 crystal growth: (a) extensively sulfided in the laboratory; (b) laboratory-sulfided following by 2 days reduction in the HDS reactor; (c) laboratory-sulfided followed by 11 days in the HDS reactor.

lowed by 2 days in the HDS reactor; and Fig. 9c, sulfided and followed by 11 days in the HDS reactor. It appears that even after completing protocol I the areas of both the Mo–S and Mo–Mo peaks continue to increase upon extended HDS treatment. It is proposed that the enhanced growth of these peaks is due primarily to continued reduction of the more stable Mo–O bonds, and to a lesser extent to migration of the molybdenum and sulfur atoms so as to generate larger and better organized crystallites of MoS_2. Correlation of these data with catalytic activity will be discussed in the accompanying paper (*2*).

OXIDE → SULFIDE REDUCTION SEQUENCE

The structural transformation which takes place during the conversion from oxide to sulfide under protocol I is illustrated in Fig. 10, which consists of Fourier transforms for time-sequences of compositions (18,0) and (18,6). These curves are not the final $D(R)$'s but are $\rho_3(R_\psi)$; i.e., the Fourier transforms after correcting for errors in background and finite range of integration, but prior to phase shift correction and multiplication by R^2. We chose $\rho_3(R_\psi)$ to present the reader with a measure of the experimentally derived intensities of the three outer peaks relative to the background noise. Figures 11a, b, c are plots of time-dependent relative areas of Mo–O, Mo–S, and Mo–Mo peaks, for (18,0). During the early stages of sulfiding, while the area under ψ decreases, peak b (Fig. 10) appears unaffected; the fate of a could not be followed due to its superposition by the Mo–S peak. On further sulfiding the Mo–S peak begins to grow and this continues until it attains its limiting value.

The presence of CoO reduces the initial conversion rate; this is apparent from Figs. 10a–d vs e–h. The Mo–S peak appears after 40 min for the (18,0) preparation, but ≈70 and ≈120 min are required for the (18,3) and (18,6) samples, respectively. As sulfiding progresses, b shifts slightly to higher R values. Even though growth of the Mo–Mo peak overlaps a major portion of b, it is still discernible as an unresolved shoulder on the low-R side of Mo–Mo. This supports our previous suggestion that peak b is due to Mo–Al scattering, which is not significantly changed by sulfiding. The area of ψ diminishes but a residual remains in the form of the split pair, β and γ. It seems that the sum of area under β and γ attains its terminal magnitude before the Mo–S and Mo–Mo peaks reach their final areas. In general, β and γ in low CoO loaded samples approach this stage earlier than those with higher CoO content. We interpret β and γ to be due to nonreducible oxygens, since these peaks are present even after extended HDS processing.

To establish a quantitative basis for estimating the extent of nonreducible oxygens, EXAFS scans were obtained of three me-

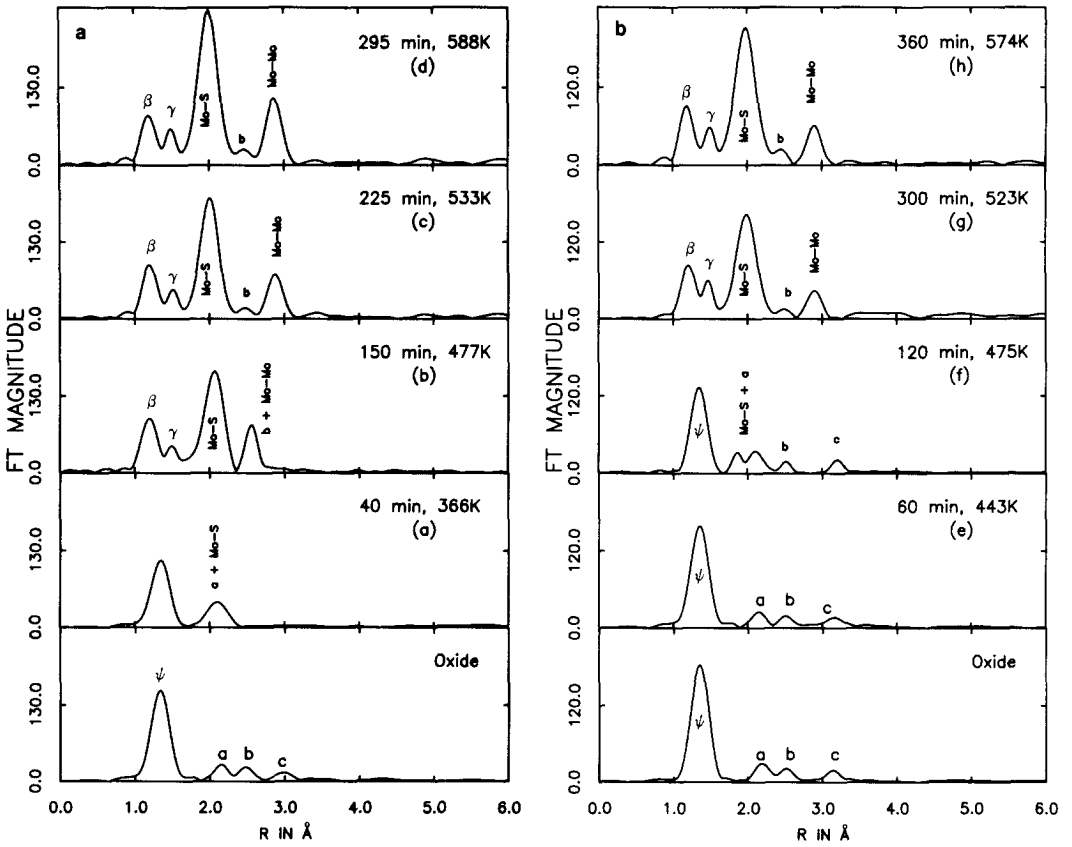

FIG. 10. $\rho_3(R_\psi)$ curves. Temperature–time conversion sequences following Protocol I. (a) Panel a → d was followed by (18% MoO_3 + 0% CoO). Panel e → h was followed by (18% MoO_3 + 6% CoO).

chanical mixtures (*m,m*) of {MoS_2/oxide-prep/Al_2O_3}. Their absorption spectra were analyzed according to our standard program. The significant parameters which characterize these $D(R)$ curves are listed in Table 1, for comparison with corresponding values obtained by superposing [after background correction] $k^3\chi(k)$ curves of MoS_2 and of the oxide preparations in proportion to their composition in the mix (computer simulation, *c,s*), and calculating its Fourier transform. The *m,m* and *c,s* curves are in general agreement with each other. The Mo–O peaks in the mixtures (*m,m* and *c,s*) appear at somewhat larger R values, and incorporate somewhat larger areas than was estimated from their compositions. Again, this is due to the difficulty of extracting a small peak, such as Mo–O in the

TABLE 1

Peak Area Calibration (Arbitrary Units)

Specimen	A(Mo–O)	A(Mo–S)	A(Mo–Mo)	$\frac{A(\text{Mo–Mo})}{A(\text{Mo–S})}$
A	243	[a]	577	—
B	—	2648	6337	2.39
c,s:	157	1641	3987	2.43
m,m 1	171	1601	3521	2.20
m,m 2	177	1590	3506	2.21
m,m 3	180	1650	3816	2.31
m,m 4	188	1701	3810	2.23

Note. A = 18% MoO_3 + 0% CoO + 82% Al_2O_3 (catalyst preparation), B = 50% MoS_2 + 50% Al_2O_3; *c,s* = 36% A + 64% B. 1 = 6.3% MoO_3 + 11.7% MoS_2 + 82% Al_2O_3. 2 = 6.7% MoO_3 + 0.56% CoO + 11.12% MoS_2 + 81.51% Al_2O_3. 3 = 6.17% MoO_3 + 1.03% CoO + 11.67% MoS_2 + 81.13% Al_2O_3. 4 = 6.3% MoOs + 2.1% CoO + 11.55% MoS_2 + 80.05% Al_2O_3.

[a] Small peaks due to Mo–O scattering with total area ≈320 (appear at 2.12–2.80 Å).

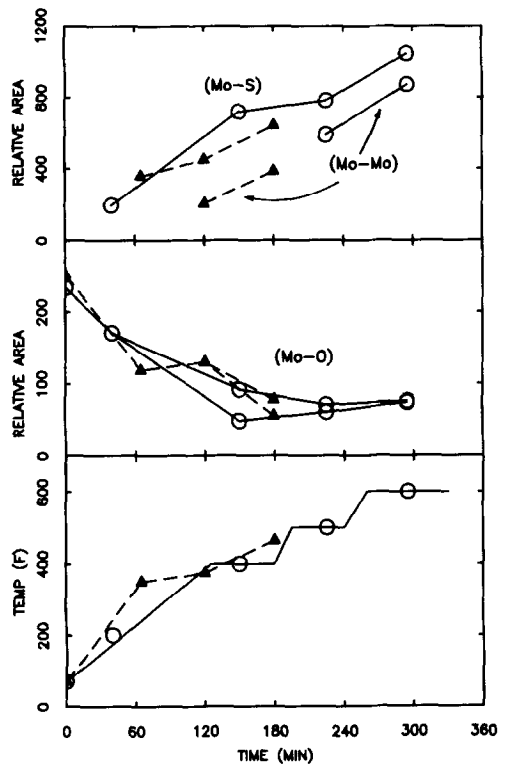

FIG. 11. Time dependence of relative areas for $D(R)$ peaks assigned to Mo–S, Mo–Mo, and Mo–O for samples reduced *in situ* according to Protocol I, for 18% MoO_3, 0% CoO. Two time-histories are displayed (full and dashed lines).

sulfided samples, from the noise due to false peaks below 1 Å, and underscores an inherent limitation of current EXAFS data reduction programs (*4*). Of particular interest is the ratio, A(Mo–Mo)/A(Mo–S) which is 2.39 in MoS_2; 2.43 in *c,s*, and 2.23 in *m,m*; it is considerably smaller in the sulfided catalysts. The Mo–Mo scattering in the residual oxide states of the catalysts contribute negligibly to the derived Mo–Mo peak.

Group II samples. The Fourier transforms of samples of this type differ in intensities but not significantly in relative peak positions from those in Group I. The area of ψ(Mo–O) decreases with increasing temperature, as expected. The first appearance of the β and γ peaks for three samples with the same MoO_3 loading depends on CoO loading, as indicated: (533°K for 18% MoO_3, 0% CoO), (533°K for 18% MoO_3, 3% CoO), and (644°K for 18% MoO_3, 6% CoO); apparently the promoter slows down the sulfiding rate, as noted above for Group I. The areas under the Mo–S and Mo–Mo peaks increase with increasing temperature. Sulfiding begins at relatively low temperatures. Fourier transforms of samples treated at 477°K for 2 h, whatever the composition, show no significant differences from those treated for 1 h only, which suggest that at this temperature a limit was reached in the maximum extent of reduction of Mo–O bonds. At that stage, the area of peak ψ was down to less than 30% of its original magnitude, but no Mo–Mo peaks were discernible, independent of the CoO loading. Mo–Mo peaks clearly appear in samples reduced at 533°K, and their areas depend on CoO loading. The relative areas of the Mo–S and the Mo–Mo peaks for the higher temperature (588 and 644°K) samples are larger than those of Group I.

No significant kinetic information could be derived from this group of experiments. We did note that Ω was higher for the 588 and 644°K preparations than those subjected to protocols I or IV. This suggests that a rapid rise in temperature during sulfiding may facilitate MoS_2 platelet growth; increased CoO loading counters this tendency to some extent.

Group III samples. No additional information was developed relative to preparations which were subjected to the full treatment. Values of Ω confirmed that: (i) a rapid rise in temperature during the H_2S/H_2 treatment enhances MoS_2 crystal growth, and (ii) this effect is greater for samples with low CoO (high MoO_3) loading compared with those with high CoO content, particularly at low temperatures. These experiments justify the empirically developed sequential step-rise program, followed in commercial practice, as mimicked by protocol I, which minimize platelet growth during sulfiding. The conversion is graphically illustrated for reduction of (18% MoO_3 + 6% CoO) at 477 and 644°K in Fig. 12.

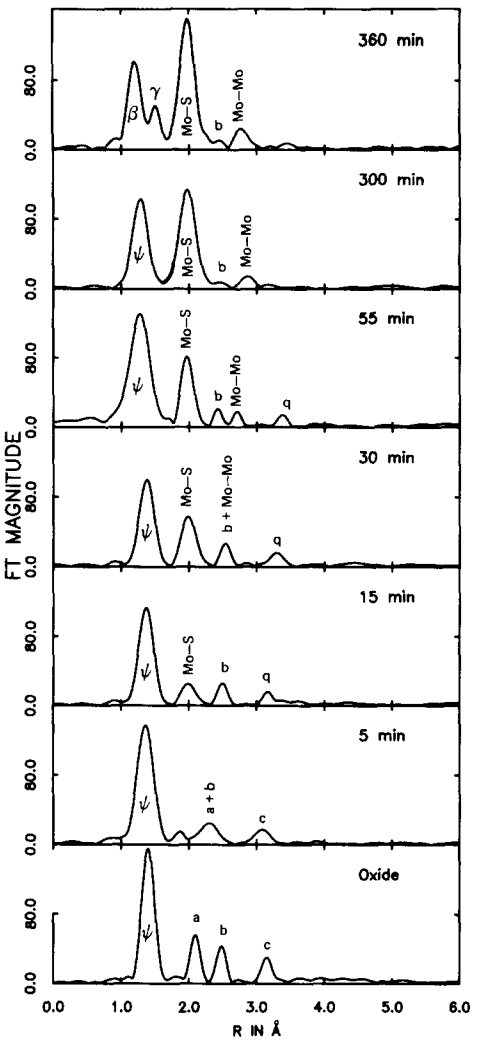

FIG. 12. $\rho_3(R_\psi)$ curves which illustrate time-dependent conversion sequences at a fixed temperature (477°K) for (18% MoO_3 + 6% CoO).

In Fig. 12 a new peak (q) appeared at 3.5–3.8 Å. It is possible that this peak is due to Mo–Mo scattering in the oxide form. At low temperatures the position of c shifted toward higher R and became q as sulfiding progressed. Eventually q disappeared. Migration of Mo atoms during the early stages may account for these shifts. When sulfiding was carried out at a higher temperature the q peak did not disappear which may indicate that on fast heating, under those conditions, the rate of forming the intermediate which is represented by q is faster than the replacement of oxygen by sulfur atoms. At low temperatures, however, the rate of forming intermediate is not as fast and peak q gradually shifted and eventually disappeared. One should recall that the areas of (β + γ) reach their limiting values during a time determined by the sulfiding temperature. Thereafter, it appears that for each temperature upon reaching their limit no further conversion of the oxide occurs without a further rise in temperature. Extended treatment at each reduction temperature enhances platelet growth.

For corresponding times and temperature the *in situ* peak areas are generally lower than for the partially sulfided samples (in the laboratory). We suspect that in the former case the catalyst temperatures lag behind the temperature of the heated block to which the specimen was attached. In contrast, in the laboratory the entire reactor was equilibrated inside a furnace. The temperature dependence is shown in Fig. 13; the upper portion is a plot of Ω values for a variety of compositions, for a 120-min treatment; the lower for a 30-min treatment.

Conversion rates derived from the time-dependent growth of the peak areas have only semiquantitative validity. Here we recorded the end product of a sequence of first-order steps: oxide → oxysulfide → sulfide → organized platelets. Regrettably these data are fragmentary. They are quite similar to reduction rates reported for NiO and CuO by H_2 (*7*). For a two-step sequence: $A \xrightarrow[k_1]{} B \xrightarrow[k_2]{} C$, one may estimate magnitudes of the rate constants from plots of the fraction converted vs log t (Powell graphs, (*8*)). We derived approximate values for k [at 477°K: 4×10^{-4} s^{-1}; at 644°K: 1×10^{-3} s^{-1}] with $0.5 < (k_2/k_1) < 1.5$. Within the precision of these measurements the rates derived from the (Mo–S) peak areas are in agreement with those derived from the resolved near-edge absorption spectra (Fig. 5).

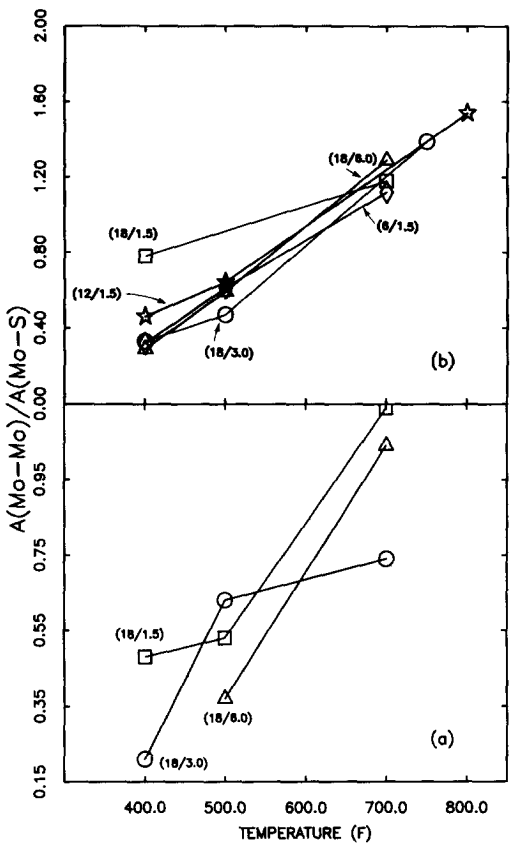

FIG. 13. The oxide → sulfide conversion for various compositions, at specified times, following Protocol III: dependence of Ω values of sulfiding temperature. Top: reaction for 120 min. Bottom: reaction for 30 min.

EXAFS STUDIES OF COMMERCIAL CATALYSTS

The following is a summary of structural changes introduced by regeneration of catalysts after extended HDS use. NALCOMO 477 with 14.9% of MoO_3 and 3.7% of CoO supported on γ-Al_2O_3, was used for the first studies. The initial samples (designated 477-S) were presulfided with the 10% H_2S/H_2 gas mixture according to the conventional program, for a total of 10 h. The amount of sulfur provided was about 2.3 times the stoichiometric requirement for a 30% MoO_3/6% CoO catalyst. Part of 477-S was regenerated and labeled 477-R. After being used in an HDS reactor for 14 days 477-R was regenerated again and labeled 477-RUR. Another sample was obtained commercially, designated XCAT, consisted of 16.1% of MoO_3 and 3.84% of CoO on a high-area alumina. It was recalcined before the test. Also, a catalyst with 18% MoO_3/3% CoO on a low-area Al_2O_3 support (194 m^2/g) was prepared to ascertain the effect of surface area; it is identified as 18-3 Low A, to distinguish it from 18-3-CATAPAL, which has the same Mo/Co composition on a larger area (289 m^2/g) base. The suffix "T" designates all catalysts after HDS activity tests.

Near-Edge Results

The location of the Mo K-edges of all samples in oxide states are in very good agreement with those of the laboratory preparations. They were found to lie within the range 7.6–8.6 eV above Mo metal. The edge positions of all the sulfided catalysts were also found to agree with the laboratory preparations (1–2 eV above the Mo metal). This indicates that the bulk oxidation states of the oxides and the sulfide catalysts are not controlled by extended HDS use or regeneration. The near-edge absorption spectra of the oxides were resolved into three Gaussians; their parameters are listed in Table 2. For comparison the near-edge parameters of two laboratory-prepared catalysts, with comparable metal loadings, are also included in the table. The Gaussian parameters for catalysts in sulfided states are quite similar to those prepared in the laboratory.

TABLE 2

Parameters of Resolved Gaussians Near-Edge Spectra of Oxide Catalysts

Identification	Mo/Co	V_1 (eV)	V_2 (eV)	V_3 (eV)	A_1	A_2	A_3
477	14.9/3.7	20002.5	20018.6	20039.2	11	38	312
477-R	14.9/3.7	2.1	18.3	38.9	11	40	311
477-RUR	14.9/3.7	2.1	18.4	39.1	11	40	315
XCAT	16.1/3.8	2.3	18.5	39.3	12	41	319
18-3-Low A	17.5/3.0	1.5	17.2	37.0	11	38	324
18-3-Catapal	17.5/3.0	2.1	18.0	37.8	11	36	332
12-3-Catapal	11.6/3.0	2.0	18.0	37.8	10	30	297

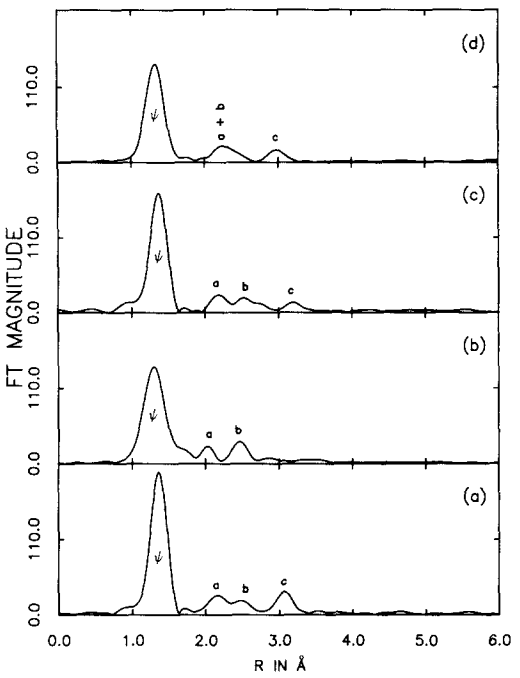

FIG. 14. $\rho_3(R_\psi)$ curves of virgin catalysts (oxide states). (a) NALCOMO—477, (b) XCAT, (c) NALCOMO—477R, (d) NALCOMO—477RUR.

Radial Distribution Curves for Catalysts in the Oxide State

Figure 14 shows plots of $\rho_3(R_\psi)$ for virgin catalysts 477 and XCAT. In the following, *qualitative* results are stated in terms of $\rho_3(R_\psi)$ curves, but unless otherwise indicated all *quantitative* results are based on $D(R)$ curves. [For graphical presentation we chose $\rho_3(R_\psi)$ curves to provide the reader with a measure of the experimentally derived peak intensities compared to the corresponding background noise.] The virgin samples in Fig. 14 have similar structures. The peak positions, as well as the *apparent* coordination numbers derived from Mo–O peak areas follow a trend close to those of the laboratory prepared samples, allowing for differences due to their various compositions. Sample XCAT has a somewhat larger FWHM for the Mo–O peak (0.36 Å compared to 0.30 Å) and the shoulder on the high-R side is more pronounced. However, its apparent coordination number (≈2.8, shoulder included) is not much different from the others. Note also that peak c, which correspond to the Mo–Mo scattering, could not be extracted from the noise, while peak a appears at a lower R. The Mo atoms in XCAT appear to be more dispersed than in the other virgin samples. The $\rho_3(R_\psi)$curves of 477-R and 477-RUR are also illustrated in Fig. 14. Obviously, regeneration of the catalysts, or their use in HDS reactors, does not introduce significant changes in their oxidic structures. The apparent coordination of Mo was reduced somewhat (<0.3), and the areas of peaks a, b, and c were also reduced upon regeneration. The peak positions of 18-3-Low A do not differ significantly from 18-3-CATAPAL. The apparent coordination of Mo, as well as the areas of peaks a and b are smaller, but the area of peak c is considerably larger than that of 18-3-CATAPAL.

Radial Distribution Curves for Catalysts in the Sulfided State

The Fourier transforms of all the sulfided catalysts have the same features as the laboratory-prepared sulfided catalysts. The two small residual Mo–O peaks appear at 1.6 and 1.9 Å, the main Mo–S peak at 2.4 Å and the Mo–Mo peak is positioned at 3.2 Å. With respect to the peak areas, A(Mo–S) of the presulfided samples agree with values obtained via laboratory sulfiding.

After HDS activity tests, both Mo–S and Mo–Mo peaks show increased areas as a consequence of MoS_2 crystal growth, but their increase in area is considerably smaller than for the comparable treatment of laboratory-prepared samples. Catalysts which have seen *extended* use for HDS before activity tests were run show larger increases in Mo–S and Mo–O areas. The significant parameters for five samples are summarized in Table 3.

DISCUSSION

That conversion of oxidic molybdenum to the sulfide upon H_2S/H_2 reduction of Co–Mo/Al_2O_3 HDS catalysts was incom-

TABLE 3

HDS Activity and RD Peak Parameters

Identification	Relative activity[a]	Catalyst area (m^2/g)	Mo–S		Mo–Mo		Ω
			Position (Å)	Area	Position (Å)	Area	
477-T	0.115	267	2.38	1537	3.18	1847	0.502
477-RT	0.113	263	2.38	1844	3.18	2335	0.529
477-RURT	0.120	257	2.38	1671	3.18	1937	0.484
XCAT-T	0.074	322	2.38	1574	3.16	1954	0.519
18-3-Low A-T	0.172	167	2.40	1965	3.18	2477	0.527

[a] Rate constant per unit area of catalyst (WHSV/SA) = $[(S_{feed})/(S_{product})]^{1-n}$; $n = 2$.

plete, has been reported by several authors (*3, 9–11*). Our studies via EXAFS directly confirm this conclusion, since residual Mo–O peaks are present in the RD curves of samples subjected to extended sulfiding. From the areas found in the calibrating spectra (Table 1) we estimate a net conversion of the order of 60% in Group I samples and approximately 70% for Group IV samples. Analyses (*2*) of Group IV samples (used for HDS) indicated that the sulfur content is less than that calculated for MoS_2 and Co_9S_8. This also supports the conclusion that conversion to the sulfides was incomplete. Sulfurization of these precatalysts at low temperatures (<477°K) and/or brief treatment at higher temperatures (≤20 min at 644°K; ≤60 min at 477°K) do not produce MoS_2 platelets. Even when Mo–S peaks do appear in the radial distribution curves, no Mo–Mo peaks are discernible under such mild sulfiding conditions. This suggests that sulfiding initially involves replacement of the more distant oxygen atoms by sulfur, with minor adjustments of spacings. A one-to-one replacement of oxygens by sulfurs at some of the more reactive bridging oxygen sites, is possible (*3, 9*). Oxygen vacancies may also form under these reducing conditions. Increasing the temperature and/or lengthening the H_2S/H_2 treatment leads to the appearance of Mo–Mo scattering contributions in the Fourier transforms, indicative of structural rearrangement. A layer of MoS_x ($x < 2$) on the surface of the support may be formed at that time. The observation that peak *b* remains in all the sulfided samples indicates that some molydenum–substrate bonds are not significantly disturbed by sulfiding. In support of this Okamoto *et al.* (*11*) and Grimbolt *et al.* (*12*) compared the Mo/Al and Co/Al XPS intensity ratios of the oxidic precatalysts with the sulfided catalysts and found that the surface structures of the Mo/Co catalysts do not alter essentially upon sulfurization. Models proposed by Massoth (*9, 13*) and Schrader and Cheng (*3, 14*) show an Mo–S surface layer which is bound extensively to the alumina by Mo–O–Al bonds. However, the extent of structure rearrangement is limited by the temperature so that for any specified set of conditions the formation of Mo–S and Mo–Mo structural units eventually slows down. Our data for Group II and Group III clearly show that the reaction temperature has a greater effect than reaction time; this is consistent with Massoth's results (*9*), that a limiting catalyst sulfur content is attained for each selected temperature. This may imply that different types of reactions are involved or that the activation energy varies with the extent of sulfidation. Pollack *et al.* (*15*) reported that upon extended use, or sulfiding at higher temperatures, recrystalli-

zation takes place. The transition of the two-dimensional MoS_x to three-dimensional MoS_2 was observed by X-ray diffraction (*15, 16*) and by high-resolution electron microscopy (*17*).

We propose that the low areas under the Mo–S and Mo–Mo peaks of the sulfided catalysts compared to those in crystalline MoS_2, measure the residual unreduced Mo–O's as well as the dispersion of the molybdenum sulfide phase. Unlike bulk MoS_2 which consists of stacked Mo and S layers, in the catalysts platelets of S_x–Mo–O_y are indicated. In bulk MoS_2, each Mo atom is surrounded by six S and six Mo, so that the ratio of peak areas should be approximately proportional to the ratio of their atomic numbers, $Z(Mo)/Z(S) = 2.625$; indeed, our EXAFS RD's show 2.4 for crystalline MoS_2. However, for all the catalyst preparations this ratio is much smaller. Thus, while Mo atoms located within large platelets have six neighboring Mo, those which reside at corners or edges have smaller numbers of neighbors so that the average is considerably below six. Our data also indicate that in the catalysts there are fewer S atoms around Mo, since not all the oxygens have been replaced by S, but overall the number of neighboring Mo's is reduced much more than S, and the ratio of peak areas (Mo–Mo)/(Mo–S) is less than 1.6, rather than 2.4. From Fig. 8 it is evident that increasing the MoO_3 loading leads to larger MoS_x platelets, whereas increasing the CoO content decreases their size. This is in agreement with interpretations of Raman spectra (*3*) to the effect that larger crystallite of MoS_2 result from higher loadings of Mo. The presence of peak *b* (Mo–substrate) in the sulfided catalysts indicates the retention of dispersion for a *fraction* of Mo's. The extent of dispersion of Mo in the oxide state is represented by the relative area of peak *c* (Mo–Mo), while for the sulfided preparations the area of the peak at ≈3.16 Å measures the ordering of Mo's in an MoS_2-type structure. Figure 8b shows that at constant Co loading this *ordering* increases with Mo content in the freshly sulfided catalysts; at constant Mo loading dispersion increases with increasing Co. In contrast, the dispersion in the oxides, as measured by the area of peak *c*, passes through a shallow maximum at total metal loading 0.15–0.20 moles per 100 g of catalyst. However, Topsøe (*6*) found that the Co promoter does not significantly change the dispersion of the MoS_2 phase. The basis for this disagreement could be the difference in sulfiding conditions. They followed a more drastic schedule, so that more extensive recrystallization occurred (4 h at 675°K). Our data for Group IV (extended use in HDS reactors) do show a weaker effect of Co on A(Mo–Mo) and hence on Ω. This explanation is also supported by our Group II data, where rapid heating at 588 and 644°K for 2 h lead to larger areas of Mo–S and Mo–Mo as well as larger Ω's compared to sulfiding for 10 h (Group I). The larger the MoS_2 crystals the lesser the dispersion effect due to the promoter.

The rate of conversion of terminal (distant) oxygens is solely dependent on the reaction temperature; catalyst composition does not affect this rate. This conclusion is based on the near-edge data, $A_3(t)$. Of course, the rate of structural rearrangement is also sensitively dependent on the temperature, but there the catalyst composition does have an effect since the different degrees of distortion in the oxidic form are controlled by the composition. High Mo and low Co content do favor rearrangement. Our experiments provide no clear evidence for the slowing down of the rate of sulfurization when MoO_3 loading is reduced, as suggested by some authors (*3, 10c*).

A quantitative formulation of the data as presented rests on two reasonable assumptions: (a) the ratio $A(\text{Mo–S})_{obs}/A(\text{Mo–S})_{MoS_2}$ is a measure of the number of Mo–S bonds generated during treatment with H_2S and with sulfur-bearing hydrocarbons in the HDS reactor (i.e., the fraction of Mo's present as Mo–S); (b) the ratio of A(Mo–

$Mo)_{obs}/A(Mo\text{–}Mo)_{MoS_2}$ measures the number of Mo–Mo pairs in platelet form, compare to those in the crystal. The calibration in Table 1 gives for $A(Mo\text{–}S)_{MoS_2}$ and $A(Mo\text{–}Mo)_{MoS_2}$, respectively, 2648 and 6337 units [arbitrary, but consistent in all our programs]. In the EXAFS data reduction procedure, for a sample which consists of a mixture of Mo–S and Mo–X pairs, the amplitude of those oscillations in the $\mu(E)$ curve which determine the area under the Mo–S radial distribution peak is normalized by the *sum of all* Mo–X background levels, so that:

$$A_y(Mo\text{–}S)_{obs} = A(Mo\text{–}S)_{MoS_2} * \frac{\text{scattering factor for (Mo–S)}}{\Sigma \text{ scattering factors for (Mo–X)}}. \quad (2)$$

This was demonstrated in Table 1.

Conversion of the oxide to the sulfided state leads to microcrystalline growth; some size distribution of platelets (possibly lognormal, (*18*) is generated. Let N_δ be the number of platelets per unit area of sulfided catalyst, with a mean linear dimension δ. Express $N_\delta = N_t \cdot g(\delta)$, where N_t denotes the total number of platelets per unit area of catalyst, and $g(\delta)$ is a normalized distribution function: $\int_0^\infty g(\delta)d\delta = 1$. Assuming that the platelets consist of a single slabs of S–Mo–S and/or O–Mo–S, the number of Mo–S pairs in a platelet of dimension δ is $n = c_1\delta^2/D$, where c_1 is a surface-shape parameter, and includes a factor for the Mo–S coordination number; D is the effective area occupied by one MoS_xO_y unit (estimated $\approx$ 12 Å^2). Hence the *total number* of Mo–S pairs (per unit volume) as recorded by EXAFS is

$$(Mo\text{–}S)_t = N_t \int_0^\infty \left(\frac{c_1\delta^2}{D}\right) g(\delta)d\delta * SA * \rho \rightarrow [Mo]\frac{A(Mo\text{–}S)}{2648}, \quad (3)$$

where SA is the surface area of catalyst/unit wt; ρ = wt/unit volume; [Mo] is the number of molybdenums per *unit volume;* and $A(Mo\text{–}S)/2648$ is the measured fraction of oxide which has been sulfided.

If all the sulfided Mo's were aggregated into a single platc (an S–Mo–S slab), the number of Mo–Mo pairs would be $(Mo\text{–}Mo)_\infty = \alpha(Mo\text{–}S)_t$, where α (somewhat <1) is a correction factor for those atoms which reside on the periphery of that relatively large plate. For a *distribution of sizes*, define $f(n) \cdot n$ as the #(Mo–Mo) which are incorporated in a platelet of dimensions δ, with $c_1\delta^2/D$ molybdenum–sulfur pairs. Thus, for sulfided catalysts, EXAFS records

$$(Mo\text{–}Mo)_t = N_t \int_0^\infty f\left(\frac{c_1\delta^2}{D}\right) * \left(\frac{c_1\delta^2}{D}\right) g(\delta)d\delta * SA * \rho \rightarrow [Mo]\frac{A(Mo\text{–}Mo)}{6337} \quad (4)$$

$$\frac{(Mo\text{–}Mo)_t}{(Mo\text{–}Mo)_\infty} = \frac{\int_0^\infty f\left(\frac{c_1\delta^2}{D}\right)\delta^2 g(\delta)d\delta}{\alpha\int_0^\infty \delta^2 g(\delta)d\delta} \rightarrow \frac{\Omega}{\alpha}. \quad (5)$$

The identity (5) follows from the definition of Ω. Thus, Ω is a measure of platelet size, since it is the ratio of pairs actually present to the number one would observe were all the Mo's collected into a single slab. A model for a single layer of hexagonal close packed sulfur atoms, with underlying molybdenums shows that for $15 < n < 50$, $0.2 < f(n) < 0.65$, a range which is consistent with the values of Ω plotted in Fig. 8c. (Ref. *19* presented diagrams of possible platelet structures and tables of corresponding metal and sulfur atom coordination types.)

For later use it is interesting to inquire how many Mo–S pairs [or Mo–Mo pairs] are located at the *rims* of the platelets. Given a linear dimension δ, that number is $\left(\frac{c_2}{W} \cdot \delta\right)$, where c_2 is a linear-shape parameter and W is an effective width of such an atom pair along the periphery of the platelct. Thus,

$$(Mo\text{–}S)_{rim} = N_t \int_0^\infty \left(\frac{c_2\delta}{W}\right) g(\delta)d\delta * SA * \rho \quad (6)$$

which is proportional to $\left\{[\mathrm{Mo}]\frac{A(\mathrm{Mo-S})}{2648}\right\}^{1/2}$. This dimensional relation is readily demonstrated, if one assumes a simple, integrable form for $g(\delta) = a^2\delta e^{-a\delta}$. Then

$$(\mathrm{Mo-S})_{\mathrm{rim}} = 2\frac{N_t c_2}{W} * SA * \rho * \frac{1}{a}, \qquad (6a)$$

whereas

$$(\mathrm{Mo-S})_t = 6\frac{N_t c_1}{D} * SA * \rho * \frac{1}{a^2} = [\mathrm{Mo}]\frac{A(\mathrm{Mo-S})}{2468}. \qquad (6b)$$

Substitution for the distribution parameter a from (6b) into (6a) leads to

$$(\mathrm{Mo-S})_{\mathrm{rim}} = \left\{\frac{2}{3}N_t\frac{c_2^2}{c_1}\frac{D}{W^2} * SA * \rho\right\}^{1/2} * \left\{[\mathrm{Mo}]\frac{A(\mathrm{Mo-S})}{2648}\right\}^{1/2}. \qquad (7)$$

One can now interpret the composition dependences shown in Figs. 8a, b, c. Since low Mo loadings in the oxidized state have higher coordination numbers, one should anticipate that low MoO_3 preparations would undergo lower conversions (i.e., more short Mo–O bonds have to be broken) as shown by the lower values of #(Mo–S) in Fig. 8a for the virgin samples. Addition of the promoter further reduces the extent of sulfiding. However, after extended HDS exposure, there is no significant dependence on metal loading. Figure 8b shows that platelet growth follows parallel trends. One should note, however, that while we have allocated the entire area of the RD peak at 3.16 Å to Mo–Mo contributions, we cannot exclude the possibility that in the virgin samples, some of the positions in the metal-atom layer are occupied by cobalt. Suppose Mo and Co were randomly distributed. For a composition $q \equiv \mathrm{Co}/(\mathrm{Co} + \mathrm{Mo})$ the peak intensity at this distance (which is essentially determined by the close packing of the S atoms in the top layer) would be proportional to $\{42(1 - q) + 27q\} = 42\{1 - 0.36q\}$. This may account in part for the decline in the areas of 3.16-Å peaks with added Co in the virgin catalysts, as initially sulfided. Then, HDS processing not only leads to larger peak areas, i.e., platelet growth, but also removes the dependence on the total metal loading (except for three low compositions). It appears that during long exposures to sulfur-containing species the Co atoms which may have been trapped in the Mo layer segregated to the peripheries of the platelets. (Ref. (*20*) presented evidence for the edge location of Co based on AEM studies of large crystals. This was further supported by their IR spectra of adsorbed NO; see also Ref. (*21*).) This will be quantified when the Co K-edge absorption spectra are fully analyzed.

Dependence of Ω values, which incorporate corrections for incomplete sulfiding, on metal loading for the virgin catalysts (Fig. 8c) supports the model that during the initial sulfiding small platelets are produced ($\Omega \approx 0.5$), possibly with some randomness in the distribution of Mo/Co within the metal layer. Extended HDS treatment leads to platelet growth (higher Ω's), and there is no dependence on Co loading which indicates that whatever Co atoms were present migrated from the molybdenum layer, most likely to the platelet edges. Equation (5) predicts that for stabilized catalysts, Ω should be independent of metal loading, as observed.

Assume that catalytic activity is primarily determined by the number of Mo–S (or Mo–Mo) pairs available at the peripheries of the rafts. Then Eq. (7) indicates that activity should be linearly dependent on $\left\{[\mathrm{Mo}]\frac{A(\mathrm{Mo-S})}{2648}\right\}^{1/2}$, but modulated by the first factor, which depend on shape parameters and Co content. This is demonstrated in the accompanying paper.

ACKNOWLEDGMENTS

This work was supported in part by the National Science Foundation under an Industry/University Co-

operative Research Program, Grant CPE-80-00025, and in part by a grant from the ARCO Petroleum Products Corporation, a division of Atlantic Richfield Company. The EXAFS spectra were recorded at the Cornell High Energy Synchrotron Source supported by NSF Grant DMR-780/267.

REFERENCES

1. Chiu, N-S., Bauer, S. H., and Johnson, M. F. L., *J. Catal.* **89,** 226 (1984).
2. Johnson, M. F. L., Voss, A. P., Bauer, S. H., and Chiu, N-S., *J. Catal.* **98,** 51 (1986).
3. Schrader, G. L., and Cheng, C. P., *J. Catal.* **80,** 369 (1983).
4. Chiu, N-S., Bauer, S. H., and Johnson, M. F. L., *J. Mol. Struct.* **125,** 33 (1984).
5. (a) Seshardi, K. S., and Petrakis, L., *J. Catal.* **30,** 195 (1973); (b) Konings, A. J. A., VanDooren, A. M., Koningsberger, D. C., De Beer, V. H. J., Farragher, A. L., and Schuit, G. C. A., *J. Catal.* **54,** 1 (1978); (c) Konings, A. J. A., Volster, A., de Beer, V. H. J., and Prins, R., *J. Catal.* **76,** 466 (1982).
6. Clausen, B. S., Topsøe, H., Candia, R., Villadsen, J., Lengeler, B., Als-Nielsen, J., and Christensen, F., *J. Phys. Chem.* **85,** 3868 (1981).
7. Boldyrev, V. V., Bulens, M., and Delmon, B., "The Control of the Reactivity of Solids," (pp. 87–98. Elsevier, New York, 1979.
8. Frost, A. A., and Pearson, R. G., "Kinetics and Mechanisms," 2nd ed., p. 170. Wiley, New York, 1963.
9. Massoth, F. E., *J. Catal.* **36,** 164 (1975).
10. (a) Schuit, G. C. A., and Gates, B. C., *AIChE J.* **19,** 417 (1973); (b) Mitchell, P. C. H., and Trifiro, F., *J. Catal.* **33,** 350 (1974); (c) de Beer, V. H. J., Bevelander, C., Van Sint Fiet, T. H. M., Werter, P. G. A. J., and Amberg, C. H., *J. Catal.* **43,** 68 (1976).
11. (a) Okamoto, Y., Nakano, H., Shimokawa, T., Imanaka, T., and Teranshi, S., *J. Catal.* **50,** 447 (1977); (b) Okamoto, Y., Imanaka, T., and Teramshi, S., *J. Catal.* **65,** 448 (1980); (c) Okamoto, Tomika, T., Katoh, Y., Imanaka, T., and Teranishi, S., *J. Phys. Chem.* **84,** 1833 (1980).
12. Grimbolt, J., Dufresne, P., Gregembre, L., and Bonnelle, J-P., *Bull. Soc. Chim. Belg.* **90,** 1261 (1981).
13. Massoth, F. E., *J. Less Common Met.* **54,** 343 (1977).
14. Schrader, G. L., and Cheng, C. P., *J. Phys. Chem.* **87,** 3675 (1983).
15. Pollack, S. S., Makovsky, L. E., and Brown, F. R., *J. Catal.* **59,** 452 (1979).
16. Topsøe, N-Y., *Bull. Soc. Chim. Belg.* **90,** 1311 (1981).
17. (a) Thomas, J. M., Millward, G. R., and Bursill, L. A., *Philos. Trans. R. Soc. London, Ser. A* **300,** 43 (1981); (b) TopsøE, H., *in* "Advances in Catalytic Chemistry II," Utah, 1982, ACS Symposium Series.
18. Wilcox, C. F., Jr., Russo, S., and Bauer, S. H., *J. Phys. Chem.* **83,** 897 (1979).
19. (a) Kasztelan, S., Toulhoat, H., Grimblot, J., and Bonnelle, J. P., *Appl. Catal.* **13,** 127 (1984). (b) Grange, P., *Catal. Rev.-Sci. Eng.* **21,** 135 (1980).
20. Sørensen, O., Clausen, B. S., Candia, R., and Topsøe, H., *Appl. Catal.* **13,** 363 (1985).
21. TopsøE, H., *et al., Bull. Soc. Chim. Belg.* **93,** 727, 783 (1984).